Chapter 18
Occurrence and Origin of Scapolite in the Neoproterozoic Lufilian–Zambezi Belt, Zambia: Evidence/Role of Brine-Rich Fluid Infiltration During Regional Metamorphism

Crispin Katongo, Friedrich Koller, Theodoros Ntaflos, Christian Koeberl, and Francis Tembo

Abstract Scapolite is an important mineral in the metamorphism of calc-silicates, marbles, amphibolites, and metagabbros in the Lufilian–Zambezi belt of Zambia. Both field and petrographic studies on granite gneisses, amphibolites, and metagabbros from the Munali hills area, in the southern part of the Lufilian–Zambezi belt indicated that scapolitization was due to metasomatism. The scapolite occurs as a pervasive replacement of plagioclase in the Munali hills granite gneiss, amphibolites, and metagabbros, and is associated with mineral assemblages that are indicative of amphibolite-facies metamorphism. Results of mineral analyses show that all the scapolites have calcian–marialite compositions, which range from 27 to 47 Me % and X_{Cl} contents of 0.37–0.50 a.p.f.u. The anorthite equivalent (31–46 EqAn %) of the scapolites overlaps with that of coexisting plagioclase (21–48 X_{An} %). The composition of scapolite is similar to that of the Copperbelt region of Zambia, where there is documented evidence of evaporite horizons. Moderate to high NaCl salinities, which range from 0.2–0.5 mol, and high contents of Cl in scapolite indicate that metamorphism in the belt was accompanied by metasomatic introduction of NaCl-rich fluids, which were derived from evaporite horizons that existed in the metasedimentary succession in the belt. This study shows that evaporites, from which NaCl-rich fluids were derived, were widespread in the Lufilian–Zambezi belt and played an important role in the metamorphic history of the belt.

C. Katongo†, F. Koller, T. Ntaflos, and C. Koeberl (✉)
Department of Lithospheric Research, University of Vienna, Althanstrasse 14, A-1090 Vienna, Austria
e-mail: friedrich.koller@univie.ac.at; theodoros.ntaflos@univie.ac.at; christian.koeberl@univie.ac.at

F. Tembo
School of Mines, Department of Geology, University of Zambia, P.O. Box 32379, Lusaka, Zambia
e-mail: ftembo@mines.unza.zm

†Deceased

J. Ray et al. (eds.), *Topics in Igneous Petrology*, DOI 10.1007/978-90-481-9600-5_18,

18.1 Introduction

The fluid evolution in metamorphic terrains may be recorded by fluid inclusions and mineral chemical equilibria. Several studies have shown that scapolite is a mineral indicator of chlorine (Cl) concentration in coexisting fluid (e.g., Orville 1975; Ellis 1978; Vanko and Bishop 1982; Oterdoom and Wenk 1983; Mora and Valley 1989; Moecher and Essene 1991; Harley et al. 1994). Unlike other chlorine-bearing minerals, such as those in the mica and amphibole groups, scapolite contains little OH; as such, its Cl content at a given pressure and temperature conditions reflects the NaCl activity in the fluid, independent of the f_{H2O}, thereby making scapolite an ideal indicator of Cl composition in the fluid (Ellis 1978). Scapolite-group minerals are generally considered as the salt-bearing analogues of (Na, Ca)-feldspars, which are stable under conditions of high volatile activity. Compositions within the scapolite group are represented generally as 3(Ab, An, Ksp).($CaCO_3$, NaCl, $CaSO_4$), where Ab, An, and Ksp refer to the components $NaAlSi_3O_8$, $CaAl_2Si_2O_8$, and $KAlSi_3O_8$, respectively (Rebbert and Rice 1997). The end-member formulae were originally derived by analogue with plagioclase and may be written as marialite (Ma) = $3NaAlSi_3O_8$. NaCl (or Ab_3. NaCl) and meionite (Me) = $3CaAl_2Si_2O_8$. $CaCO_3$ (An_3 . $CaCO_3$) (Evans et al. 1969; Teertstra and Sherriff 1997). Beside Silvialite (Si) = $3CaAl_2Si_2O_8$. $CaSO_4$ (An_3 . $CaCO_4$) Marialite and meionite are the only two currently accepted species (Bayliss 1987).

Scapolite is a common metamorphic mineral in the Lufilian–Zambezi belt. It is widespread in most marbles and calc-silicate lithologies in southern Zambia (Munyanyiwa 1985) and is also widespread in carbonate and calc-silicate rocks in central Zambia (Simpson et al. 1965; Drysdall and Stillman 1966; Katongo 1999), but rare in granitic gneisses and pelitic schists elsewhere in the belt. Small metagabbroic bodies intrusive into the supracrustal sequence in central and southern Zambia have abundant scapolite (Simpson and Stillman 1963; Vrána et al. 1975; John et al. 2003). Although rare in most granitic rocks, scapolite has been reported in granite gneisses in southern Zambia (Wilson et al. 1993; Hanson et al. 1994). In the Copperbelt region, scapolite is abundant in the Katangan metasediments, and metagabbros (Mendelsohn 1961; Cosi et al. 1992; Tembo et al. 1999).

In spite of the prevalence of scapolite in the Neoproterozoic Lufilian–Zambezi belt, good scapolite compositional data that could be used independently in regional evaluation of scapolitization are limited. Simpson et al. (1965) determined the composition of scapolite as "dipyre" ($Na_3Ca_{l4}Si_8O_{24}Cl$) from physical properties such as specific gravity, density, refractive index etc., whereas Drysdall and Stillman (1966) found the composition of scapolite as sodic-meionite (Me_{55}) by wet-chemical analyses. Munyanyiwa (1990) reported Cl-free scapolite ($Me_{60–65}$) in calc-silicates from southern Zambia, but did not present mineral data or statement of how this mineral composition was determined. Similarly Cosi et al. (1992), Hanson et al. (1994), and Wilson et al. (1993) did not provide compositional data of scapolites from their study areas in the belt. The methods used in determining compositions of scapolite in some of these studies are grossly inaccurate and cast

doubts on the reliability of the claimed compositions of scapolite. The only previous reliable scapolite compositional data (calcic marialite-$Me_{25–38}$) in the belt are those that were obtained by electron microprobe analysis (Tembo 1994).

The origin of scapolite in most metamorphic terrains is generally attributed to evaporite precursors. In the Lufilian–Zambezi belt, in spite of limited scapolite compositional constraints, NaCl-rich fluids are generally considered by most authors to have been derived from evaporite beds that were present in metasedimentary successions.

In this paper, we present the first scapolite compositional data from the Munali hills granite gneiss, amphibolites, and metagabbros from the Munali hills area, in the southern part of the Lufilian–Zambezi belt. We also attempt to evaluate the source and composition of fluids that were associated with metamorphism in the belt. We have integrated compositional data of scapolite from the Copperbelt region in the northern part of the belt (Tembo 1994) with our data to assess the regional extent of the source of fluids, which caused extensive scapolitization in the Lufilian–Zambezi belt.

18.2 Regional Geological Framework of the Lufilian–Zambezi Belt

Until recently, the Lufilian arc and the Zambezi belt (Fig. 18.1) were believed to form discrete orogenic belts separated by the Mwembeshi dislocation zone (MDZ), on the basis of presumed marked differences in metamorphic grade, structural vergence, and orogenic histories (De Swardt and Drysdall 1964; Unrug 1983; Coward and Daly 1984; Hanson et al. 1993). The MDZ is a prominent crustal-scale ENE trending shear zone across central Zambia, which is believed to extend to the northeast into Malawi and to the southwest into Namibia (De Swardt and Drysdall 1964; Coward and Daly 1984; Daly 1986; Porada 1989; Kampunzu and Cailteux 1999). Isotopic age data of key lithotectonic units, coupled with re-interpretations of the geology in the belts in Zambia and Zimbabwe, have shown that the two belts are coeval and form part of a network of Neoproterozoic-early Palaeozoic orogenic belts in central-southern Africa (e.g., Hanson et al. 1993; Dirks and Sithole 1999; Kampunzu and Cailteux 1999; Vinyu et al. 1999; Porada and Berhorst 2000; De Waele et al. 2009). The transcontinental network of belts separates the Congo and Kalahari cratons (Coward and Daly 1984; Unrug 1983; Johnson et al. 2007; De Waele et al. 2009) and formed during the reconstruction of Rodinia (Unrug 1996; Weil et al. 1998). The disposition and composition of metasedimentary rocks in the belt are regarded to indicate deposition in a rift basin (Wilson et al. 1993; Hanson et al. 1994; Porada and Berhorst 2000).

A detailed review and synthesis of the evolutionary history for much of the Lufilian–Zambezi belt was provided by Porada and Berhorst (2000). Key et al. (2001) presented the most recent comprehensive interpretation of tectono-thermal evolution of the Lufilian arc based on their work in NW Zambia. An overview of

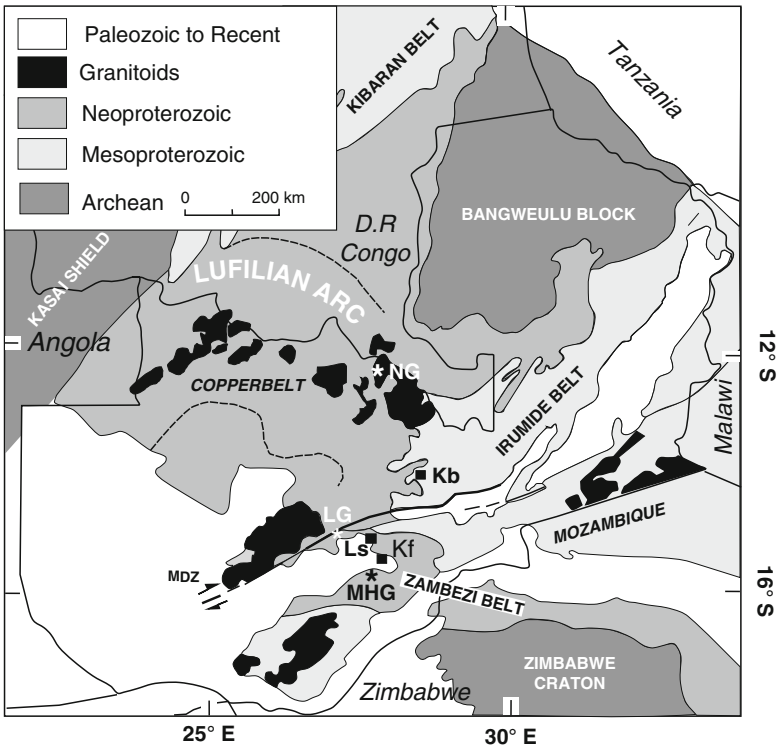

Fig. 18.1 Simplified geological map of Zambia and parts of neighbouring countries. Symbols; *: sample locations; MHG: Munali hills granite gneiss and metagabbro and amphibolitic dykes; NG: Nchanga granite; LG: Lusaka granite. Reference towns indicated by ■; Kb: Kabwe; Ls: Lusaka and Kf: Kafue (After Porada and Berhorst 2000)

the structure and geology of the Zambezi belt was given by Hanson et al. (1994). Here, we summarize previous work on the Lufilian arc and Zambezi belt to provide a regional geological framework for this study.

The Lufilian arc is an arcuate, northward convex-shaped geological structure covering eastern Angola, the southern Democratic Republic of Congo (DRC), northwestern Zambia, and is well known for its vast world-class copper–cobalt deposits (Fig. 18.1). In the Copperbelt region, which straddles northwestern Zambia and southern DRC, the stratigraphy is well known due to exploration and mining activities. The succession comprises basement and metasedimentary rocks of the Neoproterozoic Katanga Supergroup. In the Zambian Copperbelt region, the basement is composed of Lufubu schists and gneisses (Mendelsohn 1961) that are intruded by Eburnian (ca. 2,200–1,800 Ma) granites (Cahen et al. 1984). Key et al. (2001) dated basement rocks of Archaean age (ca. 2.6 Ga) in the western arm of the Lufilian arc. Overlying the Lufubu schists and gneisses, is a sequence of schists and quartzites of the Muva Supergroup, which are in turn intruded by early Neoproterozoic granites (e.g., Nchanga granite). The revised lithostratigraphy of

the Katanga Supergroup (Porada and Berhorst 2000) consists, in stratigraphic succession, of arenaceous Roan Group, carbonaceous Mwashia Group with metavolcanic interbeds, and conglomeratic Kundelungu Group. It has long been observed by many authors that there are several horizons of evaporites in the Katangan succession (e.g., Mendelsohn 1961; Binda 1994; Cailteux et al. 1994). The former existence of evaporites in the Katangan metasediments is indicated by sabkha facies, crystals and pseudomorphs of gypsum and anhydrite, stratigraphic gaps underlain by collapse breccias, chloride inclusions in ores, and saline springs (Porada and Berhorst 2000; Jackson et al. 2003). Evaporites have played an important role in deformation (Cailteux and Kampunzu 1995) and formation of megabreccias (olistostromes)(Wendorff 2000) in the Katanga succession. In the Damara belt, the southwestern extension of the Lufilian arc, former evaporite deposits are characterized by high sodium contents, abundant albite pseudomorphs after evaporite minerals and concordant collapse breccia (Porada and Berr 1988).

Metamorphism in the Lufilian arc increases gradually from prehnite–pumpellyite facies in the northern boundary of the Lufilian arc, up to amphibolite facies in the southern part of the Copperbelt region (Kampunzu and Cailteux 1999), but higher grades of up to eclogite facies have been locally recorded (Vrána et al. 1975; Cosi et al. 1992). From studies of mineral associations and phengite compositions in the ore-shale, in the Copperbelt region of Zambia, Moine et al. (1986) estimated the metamorphic conditions of 420–550°C and 2–6 kbar in the Copperbelt region. Deformation in the Lufilian arc mainly involved thin-skinned tectonics with northerly directed thrusting (Coward and Daly 1984; Daly 1986; Kampunzu and Cailteux 1999; Porada and Berhorst 2000; Key et al. 2001).

The east-west trending Zambezi belt stretches from central Zambia into northern Zimbabwe, where it merges with the north–south trending Mozambique belt (Fig. 18.1). In Zambia, the Zambezi belt consists of wide zones of remobilized Mesoproterozoic to Neoproterozoic crystalline basement, unconformably overlain by late Neoproterozoic supracrustal rocks (Hanson et al. 1988; Wilson et al. 1993). The Basement is composed of the Mpande gneiss, a megacrystic, K-feldspar, biotite augen gneiss and the Ngoma gneiss, a protomylonitic, K-feldspar gneiss. The two gneissic units form an extensive terrain in the central parts of the belt. The Munali hills granite gneiss is a small lensoidal body that is intrusive into the Mpande gneiss, and adjacent metasedimentary rocks (Smith 1963) Katongo et al. (2004) report an U–Pb zircon age of 1,090.1 ±1.3 Ma. The supracrustal sequence starts with a thick pile of rift-related bimodal volcanics, which are overlain by a thick sequence of psammites and pelites that are in turn succeeded by an extensive unit of marbles and calc-silicates rocks (De Swardt and Drysdall 1964; Wilson et al. 1993; Hanson et al. 1994). The supracrustal sequence in the Zambezi belt in Zambia has been correlated based on structural continuity and broad lithological similarities with the Makuti and Rushinga Groups in Zimbabwe (Broderick 1981; Barton et al. 1991). Evaporite horizons have not really been observed in the Zambezi belt, but former evaporites are indicated by relict chicken-wire structures, reflecting replacement of original anhydrite nodules by calcite in marbles at Nampundwe Mine, in central-southern Zambia (Burnard et al. 1993). Metamorphism in the Zambezi belt was primarily amphibolite

facies (Barton et al. 1991; Hanson et al. 1994; Hargrove et al. 2003), but locally there are occurrences of tectonically exhumed high-pressure rocks comprising eclogites and talc-kyanite whiteschists in Zambia and northwest Zimbabwe (Vrána et al. 1975; Dirks and Sithole 1999; Johnson and Oliver 2000). Diopside-plagioclase assemblages are uniformly developed in the calc-silicate rocks and carbonate formations in southern Zambia. Garnet-biotite thermometry and plagioclase-hornblende thermobarometry on amphibolite layers in the Carbonate Formations indicate peak metamorphic conditions of 560–600°C and 5–6 kbars (Munyanyiwa and Hanson 1988; Munyanyiwa 1990). These P-T conditions are consistent with widespread occurrence of kyanite in the supracrustal sequence south of Kafue. Temperatures between 565°C and 580°C and pressures ranging from 6 to 8 kbars were indicated by the garnet–hornblende thermobarometry on garnet amphibolites in the Chisamba area north of Lusaka (Katongo 1999). Occurrences of several small bodies of eclogite (Vrána et al. 1975; Vrána 1978), and talc-kyanite-whiteschists (Vrána and Barr 1972; Cosi et al. 1992; John et al. 2003) indicate that local medium to high pressure were attained during metamorphism in most parts of the Zambezi belt. Scapolite metamorphism also affected metagabbros, and eclogites in the southeastern extension of Zambezi belt in northern Zimbabwe (Dirks and Sithole 1999; Munyanyiwa et al. 1997). In contrast, to the Lufilian arc, deformation in the Zambezi belt is characterised by thick-skinned tectonics, involving both supracrustal and basement rocks (Coward and Daly 1984).

18.3 Field Relations and Petrography of Scapolite Bearing Rocks

In this study, scapolite was identified in the Munali hills granite gneiss, amphibolites, and metagabbros in the Munali hills area (Fig. 18.1). Scapolite occurs as pervasive replacement of plagioclase in all the studied lithologies, as shown in microphotos (Fig. 18.2) and field occurrences (Fig. 18.3).

18.3.1 Munali Hills Granite Gneiss

The Munali hills granite gneiss forms a small part of the Munali hills, a WNW trending elongate ridge, underlain mainly by granitic gneiss of the Mpande Formation (Smith 1963; Mallick 1966). The southern boundary of the granite gneiss is marked by an alternating sequence of kyanite schist, quartzite, calc-silicates, and marbles. The Munali hills granite gneiss is a porphyritic K-feldspar-rich granite gneiss composed of a range of fine- to coarse-grained varieties, varying from leucocratic to melanocratic types and displaying variable degrees of deformation. The granite gneiss is composed of pink microcline porphyroclasts set in fine-medium grained felsic groundmass. Isolated, dark, medium-grained irregularly

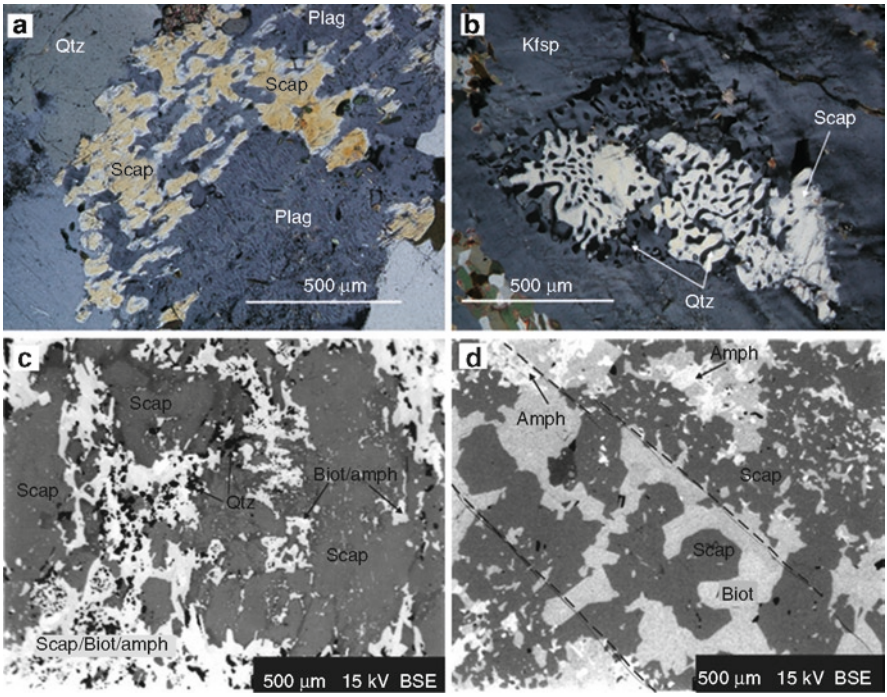

Fig. 18.2 (**a**) Photomicrograph showing characteristic partial replacement of plagioclase by scapolite in sample MHG2. (**b**) Photomicrograph showing of coronal intergrowth of scapolite and quartz in sample MHG9. Note: photograph was taken with quartz in partial extinction to enhance contrast against scapolite. (**c**) Back-scattered electron (BSE) image of coarse porphyroblastic scapolite with inclusions of quartz, biotite, and amphibole. (**d**) NW trending veinlet in central part of BSE image of relatively coarse-grained intergrowth of scapolite and biotite. Scap: scapolite; Biot: Biotite; Amp: amphibole; qtz: quartz; Plag: plagioclase: Kfsp: K-feldspar

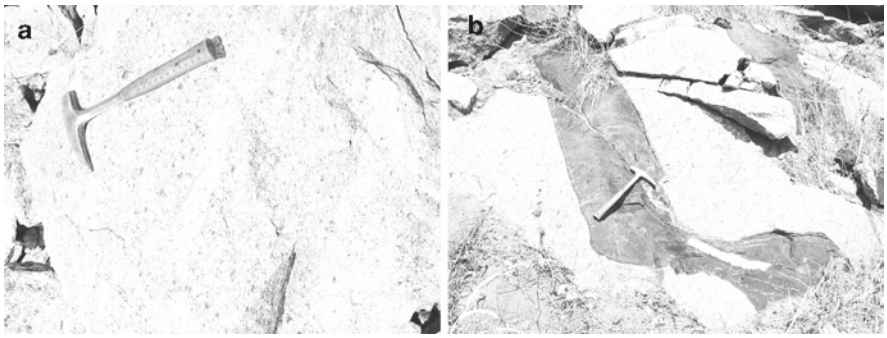

Fig. 18.3 Field pictures of the scapolite-bearing rocks in the Kafue area. (**a**) Leukocratic, medium- to fine-grained variety of the Munali Hill granite, dark spots are biotite-rich areas. (**b**) Deformed mafic dyke (now amphibolite) intruding into a medium-grained Munali Hill granite

shaped, biotite-rich enclaves are common. Deformation is generally weak, and exhibited by a crude foliation defined by aligned biotite warping around slightly elongated porphyroclasts of feldspar and quartz aggregates. The gneisses are composed of microcline, quartz, plagioclase/scapolite, biotite and calcite ± muscovite. The microcline crystals are generally poikiloblastic, hosting smaller grains of other mineral constituents, non-perthitic and slightly kaolinized. Accessory minerals include sphene, epidote, apatite, zircon, and ±tourmaline.

The granite displays varying degrees of alteration, ranging from chloritization of biotite, sericitization and ubiquitous scapolitization of plagioclase. Scapolite constitutes up to 30 modal % and invariably intergrown with plagioclase. The replacement of plagioclase by scapolite is mainly along grain margins, cleavage planes and less commonly in the cores (Fig. 18.2a). In some grains, scapolite hosts fine inclusions of twinned plagioclase, sericite, epidote, and carbonate, probably indicating replacement after slight retrogression of plagioclase. In a few porphyroblasts of scapolite, calcite occurs along cleavage or fractures planes. A few grains of scapolite display symplectite-like intergrowths with quartz (Fig. 18.2b). Undulose extinction in quartz, kink bands in biotite and deformation twins in plagioclase indicate low temperature deformation.

18.3.2 Amphibolites

The Munali hills granite gneiss is intruded by several steep, WNW trending amphibolitic dykes, measuring up to 5 m in width. At outcrop scale, the amphibolitic dykes exhibit a strong shear fabric, suggesting emplacement in extensional shear fractures. The amphibolites are dark green, and fine-grained, with white plagioclase phenocrysts and scapolite porphyroblasts, and are composed mainly of blue green amphibole and subordinate biotite, plagioclase, scapolite and minor calcite. Plagioclase is partly retrogressed to sericite. The scapolite is up to 40 modal % and partially or completely replaces plagioclase. Scapolite in the amphibolite displays various textures ranging from large porphyroblasts to fine grains and coarse-grained veinlets (Fig. 18.2c, d). The veinlets are composed of coarse-grained scapolite and biotite in stable equilibrium. Most scapolite crystals host inclusions of plagioclase, calcite, and epidote. Accessory minerals include epidote, sphene, carbonates, and opaque minerals. The opaque minerals are chalcopyrite and pyrite.

18.3.3 Metagabbros

18.3.3.1 Munali Hills Area

The metagabbro is one of the varieties of a metagabbroic composite body that is associated with nickel sulphide mineralization. The sulphide mineralization consists mainly of pyrrhotite with lesser amounts of pyrite, pentlandite, chalcopyrite, and accessory magnetite. The metagabbro is dark green, medium- to coarse-grained

and consists mainly of amphiboles, augite, plagioclase, and biotite, which have undergone various degrees of alteration. Plagioclase (20–30 modal %) is invariably partly replaced by scapolite. Other secondary minerals include chlorite, tremolite, epidote, sericite and zoisite.

18.3.3.2 Copperbelt Region

Detailed descriptions of metagabbros in the Copperbelt region are provided by Tembo et al. (1999). The metagabbros are composed of calcic amphiboles, sodic plagioclase, and variable amounts of scapolite and have preserved primary igneous textures. The metagabbros are invariably affected by hydrothermal alteration. As in other scapolite bearing rocks in the Munali hills area, scapolite in these metagabbros occurs as a pervasive replacement of plagioclase. Textural relationships among the minerals in the metagabbros indicate that scapolitization post-dated amphibolitization (Tembo 1994).

18.4 Analytical Procedures

Mineral analyses on scapolite, and associated minerals such as plagioclase, amphiboles, and biotite from a few selected samples, were conducted on a four-spectrometer CAMECA SX100 microprobe at the University of Vienna, Department of Geological Sciences. Counts were obtained simultaneously from four spectrometers, using a 15 keV accelerating voltage, a 1–2 μm beam diameter, and a beam current of 20 nA. Natural and synthetic standards were used for calibrations and the PAP correction (Pouchou and Pichoir 1991) was applied to the data.

Mineral compositional data of scapolite by Tembo (1994) from the Copperbelt region were obtained on a scanning electron microscope (SEM)-Cambridge Stereoscan 250 MK3-equipped with an energy dispersive (ED) analytical system, at the University of Göttingen, Germany. Operating conditions for the quantitative analyses were 15 keV accelerating potential, 20 nA probe current and 100 s counting time. Natural and synthetic standards were used to calibrate the analyses. Matrix effects on elements and their oxides weight percentages were corrected for and calculated using the Cambridge online program MACRO ZAF. Representative results of mineral analyses are presented in Tables 18.1–18.5.

18.5 Results

18.5.1 Scapolite

Scapolite compositions are commonly reported in terms of equivalent anorthite content (EqAn = 100 * (Al – 3)/3), where Al is calculated on the basis of tetrahedral 16 cations (Evans et al. 1969; Teertstra and Sherriff 1997), mole fractions of chlorine (X_{Cl} = Cl

Table 18.1 Representative mineral compositions of scapolite from the Munali hills area

	Munali hills granite gneisses												
	MHG2					MHG9					MHG10		
Sample													
	1r	2c	4r	5c	6r	2c	4c	5c	6c	8c	5r	6r	7r
SiO_2	53.40	53.10	53.50	53.60	54.10	52.90	53.00	53.40	52.50	52.80	57.10	56.70	55.00
TiO_2	0.03	<0.02	<0.02	<0.02	0.02	<0.02	<0.02	0.03	0.04	<0.02	<0.02	0.02	0.02
Al_2O_3	25.00	24.80	25.30	25.10	25.50	25.20	25.40	24.90	25.30	25.20	23.70	23.50	24.40
FeO	0.12	0.12	0.12	0.12	0.18	0.12	0.06	0.10	0.08	0.36	0.05	<0.02	0.04
MnO	0.05	0.02	<0.02	0.03	0.03	0.03	0.05	0.02	0.02	<0.02	<0.02	<0.02	<0.02
MgO	<0.02	<0.02	<0.02	<0.02	0.02	<0.02	<0.02	<0.02	<0.02	<0.02	<0.02	<0.02	<0.02
CaO	10.10	9.90	10.00	9.80	9.50	10.50	10.80	10.20	11.20	10.70	5.90	6.60	8.10
Na_2O	7.50	8.10	8.00	8.40	7.00	7.80	7.40	7.80	7.50	7.50	9.70	9.90	9.10
K_2O	0.78	0.84	0.71	0.71	0.64	0.69	0.70	0.77	0.84	0.73	0.92	0.85	0.81
Cl	1.75	1.86	1.79	1.95	1.76	1.73	1.73	1.84	1.61	1.78	2.60	2.50	2.38
Total	98.73	98.75	99.44	99.71	98.75	98.98	99.14	99.06	99.09	99.08	99.97	99.45	99.85
Si	7.735	7.745	7.705	7.733	7.711	7.685	7.672	7.739	7.648	7.679	8.057	8.060	7.888
Al	4.265	4.255	4.295	4.267	4.289	4.315	4.328	4.261	4.352	4.321	3.943	3.940	4.112
Ti	0.006	0.003	0.001	<0.001	0.003	<0.001	<0.001	0.006	0.008	0.001	<0.001	0.004	0.005
Fe	0.015	0.014	0.014	0.015	0.022	0.014	0.007	0.012	0.010	0.044	0.006	0.004	0.004
Mn	0.006	0.002	0.001	0.003	0.003	0.004	0.006	0.002	0.002	<0.001	<0.001	0.000	<0.001
Mg	<0.001	<0.001	<0.001	<0.001	0.004	0.001	<0.001	<0.001	<0.001	<0.001	<0.001	0.000	<0.001
Ca	1.567	1.554	1.543	1.510	1.452	1.626	1.675	1.578	1.742	1.670	0.893	1.002	1.243
Na	2.112	2.282	2.235	2.359	1.930	2.182	2.073	2.190	2.116	2.107	2.654	2.560	2.530
K	0.144	0.156	0.130	0.131	0.116	0.127	0.130	0.142	0.157	0.136	0.165	0.154	0.149
Cl	0.422	0.450	0.429	0.468	0.416	0.415	0.415	0.444	0.390	0.430	0.609	0.590	0.566
Me %	42.6	40.5	40.8	39.0	42.9	42.7	44.7	41.9	45.2	44.2	25.2	28.1	33.0
EqAn	0.422	0.418	0.432	0.422	0.430	0.438	0.443	0.420	0.451	0.440	0.314	0.313	0.371

	Amphibolites											Metagabbro		
	MHG5a			MHG5c								NDG		
Sample														
	1c	2c	4c	1c	2c	3c	4c	5c	6c	7c	8c	2c	3r	4r
SiO_2	52.90	52.90	52.70	52.96	53.40	52.90	53.00	53.20	53.00	52.90	53.10	51.70	54.70	55.00
TiO_2	<0.02	<0.02	<0.02	0.07	0.04	0.04	<0.02	<0.02	<0.02	0.02	<0.02	<0.02	<0.02	<0.02
Al_2O_3	25.41	25.30	25.30	25.18	25.50	25.10	25.00	24.90	25.00	25.00	24.60	25.90	24.20	24.10
FeO	0.06	0.26	0.26	0.25	0.50	0.38	0.29	0.15	0.21	0.15	0.09	0.14	0.19	0.11
MnO	<0.02	0.04	<0.02	<0.02	<0.02	<0.02	<0.02	0.02	<0.02	0.03	<0.02	0.04	<0.02	<0.02
MgO	<0.02	<0.02	<0.02	<0.02	<0.02	<0.02	<0.02	<0.02	<0.02	<0.02	<0.02	<0.02	<0.02	<0.02
CaO	11.10	10.80	10.80	10.45	10.20	10.60	10.50	10.10	10.60	10.40	10.10	11.30	8.20	8.00
Na_2O	7.40	7.30	7.80	7.79	7.50	7.80	8.00	8.10	7.80	7.70	8.10	7.60	9.30	9.60
K_2O	0.56	0.59	0.72	0.68	0.78	0.76	0.64	0.70	0.65	0.81	0.78	0.40	0.50	0.44
Cl	1.71	1.70	1.71	1.79	1.93	1.82	1.83	1.94	1.79	1.92	1.90	1.69	2.30	2.27
Total	99.16	98.91	99.30	99.18	99.85	99.41	99.28	99.11	99.06	98.93	98.68	98.77	99.40	99.52
Si	7.665	7.670	7.665	7.690	7.684	7.695	7.709	7.729	7.714	7.704	7.764	7.548	7.886	7.914
Al	4.335	4.330	4.335	4.310	4.316	4.305	4.291	4.271	4.286	4.296	4.236	4.452	4.114	4.086
Ti	<0.001	0.003	<0.001	0.014	0.008	0.008	0.003	<0.001	0.002	<0.001	0.003	0.001	0.002	<0.001
Fe	0.007	0.032	0.032	0.030	0.061	0.046	0.035	0.018	0.025	0.025	0.011	0.018	0.023	0.013
Mn	0.001	0.005	<0.001	<0.001	<0.001	0.001	<0.001	0.003	<0.001	0.001	<0.001	0.005	<0.001	<0.001
Mg	0.002	0.003	0.002	0.003	<0.001	<0.001	0.003	<0.001	<0.001	<0.001	<0.001	<0.001	<0.001	<0.001
Ca	1.716	1.671	1.686	1.626	1.578	1.655	1.629	1.573	1.663	1.610	1.582	1.770	1.270	1.236
Na	2.074	2.051	2.184	2.194	2.100	2.201	2.267	2.279	2.212	2.263	2.295	2.156	2.606	2.665
K	0.104	0.109	0.134	0.126	0.144	0.141	0.118	0.129	0.120	0.122	0.146	0.075	0.092	0.081
Cl	0.411	0.410	0.413	0.431	0.461	0.440	0.442	0.469	0.433	0.457	0.463	0.409	0.550	0.543
Me %	45.3	44.9	43.6	42.6	42.9	42.9	41.8	40.8	42.9	41.6	40.8	45.1	32.8	31.7
EqAn	0.361	0.361	0.361	0.359	0.360	0.359	0.358	0.356	0.357	0.358	0.353	0.484	0.371	0.362

Oxides in wt%, calculation based on 32 oxygens, Me % = 100 * (Ca/(Ca + Na), EqAn = (Al − 3)/3

Table 18.2 Representative mineral composition of scapolite from metagabbros in the Copperbelt region, Zambia (After Tembo 1994)

	Metagabbros																
Sample	FTK64				FTK44					FTK47				NN44			
	1c	1b	2a	3c	1b	2r	3c	3r	5r	1	2	4	5	1c	2r	3c	5r
SiO_2	55.69	55.18	55.06	55.81	54.00	54.58	53.45	54.12	53.87	54.16	54.34	54.28	54.61	55.02	55.06	54.87	55.60
Al_2O_3	22.59	22.72	22.99	22.62	23.45	23.23	23.56	22.95	23.14	23.22	23.20	24.02	23.63	22.81	22.94	23.19	22.79
CaO	7.42	8.42	7.73	7.60	9.47	8.93	9.75	8.95	9.20	9.00	8.83	8.94	9.10	8.74	9.04	9.09	8.12
Na_2O	9.50	8.85	9.32	9.90	8.68	8.50	8.56	8.91	8.50	8.40	8.30	8.57	8.44	9.17	8.65	8.69	9.09
K_2O	0.47	0.34	0.45	0.39	0.32	0.20	0.14	0.27	0.30	0.89	0.81	1.06	0.97	0.36	0.42	0.34	0.45
Cl	3.16	3.04	3.21	3.24	2.55	2.76	2.46	2.61	2.69	3.01	2.81	3.12	3.05	2.72	2.71	2.59	2.84
CO_2	0.47	0.52	0.46	0.47	<0.01	<0.01	<0.01	<0.01	<0.01	0.32	0.61	<0.01	0.20	0.17	0.19	0.20	0.09
SO_4	0.83	0.94	0.78	0.75	1.81	1.58	1.90	1.71	1.61	0.81	0.67	1.17	0.97	1.39	1.39	1.52	1.37
Total	99.26	99.31	99.27	100.03	99.69	99.15	99.25	98.92	98.69	98.31	98.35	99.27	99.30	98.36	98.39	98.37	98.98
Si	8.12	8.08	8.04	8.12	7.94	7.99	7.90	8.00	7.97	7.97	7.98	7.89	7.95	8.06	8.05	8.01	8.09
Al	3.89	3.92	3.96	3.88	4.06	4.01	4.10	4.00	4.03	4.03	4.02	4.11	4.05	3.94	3.95	3.99	3.91
Ca	1.16	1.32	1.21	1.19	1.49	1.40	1.54	1.42	1.46	1.42	1.39	1.39	1.42	1.37	1.42	1.42	1.27
Na	2.69	2.51	2.64	2.79	2.47	2.41	2.45	2.55	2.44	2.40	2.39	2.42	2.38	2.61	2.45	2.46	2.56
K	0.08	0.06	0.08	0.07	0.06	0.04	0.03	0.05	0.06	0.17	0.15	0.20	0.18	0.07	0.08	0.06	0.09
Cl	0.78	0.76	0.79	0.80	0.64	0.69	0.62	0.65	0.67	0.75	0.70	0.77	0.75	0.67	0.67	0.64	0.70
CO_2	0.05	0.06	0.05	0.05	<0.01	<0.01	<0.01	<0.01	<0.01	0.09	0.17	<0.01	0.06	0.05	0.05	0.06	0.03
SO_4	0.17	0.19	0.16	0.15	0.36	0.32	0.38	0.35	0.33	0.16	0.13	0.23	0.19	0.28	0.28	0.30	0.27
Me %	30.1	34.5	31.4	29.9	37.6	36.7	38.6	35.8	37.4	37.2	36.8	36.5	37.4	34.4	36.7	36.6	33.2
EqAn	0.30	0.31	0.32	0.29	0.35	0.34	0.37	0.33	0.34	0.34	0.34	0.37	0.35	0.31	0.32	0.33	0.30

Oxides in wt%, calculation based on 32 oxygens, Me % = 100 * (Ca/(Ca + Na), EqAn = (Al − 3)/3

Table 18.3 Representative mineral compositions of plagioclase from the Munali hills area

	Munali hills granite gneiss										Amphibolite		Lusaka granite		Nchanga granite	
Sample	MHG2					MHG9					MHG5a		LG2		NG4	
	1	3	4	5	6	1	2	4	5	6	5	7	1	2	2	3
SiO_2	62.00	61.10	62.00	62.40	60.70	58.30	60.20	58.80	58.20	58.10	51.80	58.20	65.10	65.10	67.40	63.90
TiO_2	<0.02	<0.02	<0.02	<0.02	0.01	0.01	0.02	0.02	0.01	<0.02	0.10	0.04	0.01	<0.02	<0.02	<0.02
Al_2O_3	25.00	25.20	24.60	25.00	25.80	26.90	25.30	26.60	26.90	26.90	30.80	26.60	21.90	22.20	21.20	22.90
FeO	0.07	0.04	0.02	0.34	0.17	0.06	0.30	0.43	0.11	0.12	0.37	0.25	0.03	0.04	0.03	0.02
MnO	<0.02	<0.02	<0.02	<0.02	<0.02	<0.02	<0.02	<0.02	<0.02	<0.02	0.02	<0.02	0.02	<0.02	<0.02	0.02
MgO	<0.02	<0.02	<0.02	<0.02	<0.02	<0.02	0.02	<0.02	<0.02	<0.02	0.11	<0.02	<0.02	<0.02	<0.02	<0.02
CaO	5.30	5.50	5.00	5.10	6.50	7.60	5.80	7.40	7.80	8.00	12.60	8.20	2.80	3.10	0.76	3.40
Na_2O	8.60	8.50	9.00	9.10	8.30	7.40	8.50	7.50	7.40	7.40	4.30	6.90	10.20	10.00	10.50	9.60
K_2O	0.07	0.10	0.17	0.09	0.07	0.20	0.11	0.13	0.06	0.11	0.17	0.05	0.16	0.18	0.08	0.08
Total	101.04	100.46	100.80	102.04	101.55	100.48	100.25	100.89	100.48	100.63	100.27	100.24	100.22	100.62	99.97	99.92
Si	10.890	10.800	10.922	10.880	10.661	10.390	10.704	10.434	10.371	10.362	9.393	10.388	11.453	11.412	11.761	11.282
Al	5.163	5.250	5.104	5.128	5.333	5.647	5.292	5.560	5.647	5.633	6.570	5.600	4.534	4.582	4.355	4.751
Ti	<0.001	<0.001	<0.001	<0.001	0.002	0.001	0.002	0.002	0.001	<0.001	0.013	0.005	0.002	<0.001	<0.001	<0.001
Fe	0.011	0.005	0.003	0.049	0.025	0.008	0.044	0.063	0.017	0.018	0.057	0.037	0.005	0.005	0.004	0.003
Mn	<0.001	0.001	0.001	<0.001	<0.001	<0.001	0.001	0.002	<0.001	0.003	0.003	<0.001	0.002	<0.001	<0.001	0.003
Mg	<0.001	0.002	<0.001	0.001	<0.001	0.002	0.005	0.004	<0.001	0.001	0.029	0.001	<0.001	<0.001	<0.001	<0.001
Ca	0.989	1.035	0.938	0.947	1.229	1.442	1.114	1.410	1.488	1.517	2.449	1.576	0.527	0.574	0.143	0.637
Na	2.912	2.921	3.083	3.075	2.809	2.542	2.933	2.583	2.549	2.553	1.526	2.374	3.475	3.407	3.558	3.298
K	0.016	0.023	0.039	0.019	0.016	0.045	0.026	0.028	0.014	0.024	0.040	0.012	0.037	0.041	0.019	0.018
Cations	19.983	20.038	20.084	20.097	20.075	20.073	20.120	20.083	20.082	20.106	20.080	19.993	20.032	20.018	19.842	19.992
X_{An}	25.2	26	23.1	23.4	30.3	35.8	27.4	35.1	36.7	37.1	61	39.8	13	14.3	3.8	16.1

Oxides in wt%, calculation based on 32 oxygens, $X_{An} = 100 * (Ca/(Ca + Na + K)$

Table 18.4 Representative mineral compositions of amphiboles in amphibolites from the Munali hills area

	Amphiboles													
Sample	MHG5a					MHG5c								
	1	2	4	5	6	1	2	3	4	5	6	7	8	9
SiO_2	38.28	38.3	38.58	38.35	38.49	38.79	38.73	38.49	39.07	38.85	38.67	38.86	38.78	38.24
TiO_2	0.64	0.56	0.73	0.63	0.67	0.59	0.45	0.42	0.43	0.55	0.42	0.59	0.47	0.56
Al_2O_3	15.27	14.7	15.15	14.47	14.82	14.19	13.92	14.03	13.83	13.86	13.97	13.69	13.94	14.28
FeO	22.77	23.38	23.46	22.84	23.15	21.94	22.44	22.45	22.18	21.86	22.53	22	21.96	22.32
MnO	0.27	0.29	0.29	0.28	0.28	0.21	0.21	0.18	0.2	0.19	0.16	0.21	0.2	0.18
MgO	5.04	5.04	5.33	5.31	5.27	6.86	6.73	6.67	7.09	6.91	6.48	7	6.87	6.57
CaO	11.31	11.33	11.23	10.98	11.46	11.74	11.7	11.63	11.53	11.61	11.77	11.73	11.76	11.65
Na_2O	1.23	1.2	1.28	1.2	1.36	1.1	1.12	1.12	1.06	1.08	1	1.07	1.08	1.1
K_2O	1.49	1.49	1.59	1.55	1.51	2.27	2.03	2.06	1.97	2.02	1.97	2.08	1.94	2.24
Cl	1.01	0.99	0.99	1	0.99	1.43	1.39	1.4	1.29	1.33	1.44	1.36	1.27	1.52
Total	97.31	97.28	98.63	96.61	98	99.12	98.72	98.45	98.65	98.26	98.41	98.59	98.27	98.66
Si	5.980	5.995	5.946	6.031	5.984	5.968	5.978	5.958	6.000	6.006	5.993	5.995	5.989	5.925
Al^{IV}	2.020	2.005	2.054	1.969	2.016	2.032	2.022	2.042	2.000	1.994	2.007	2.005	2.011	2.075
Al^{VI}	0.789	0.706	0.696	0.710	0.696	0.539	0.507	0.516	0.501	0.528	0.536	0.483	0.525	0.532
Fe^{3+}	0.525	0.613	0.650	0.597	0.553	0.654	0.746	0.762	0.810	0.700	0.733	0.719	0.727	0.711
Ti	0.075	0.065	0.085	0.074	0.079	0.068	0.052	0.049	0.050	0.064	0.049	0.069	0.055	0.065
Mg	1.175	1.176	1.225	1.245	1.221	1.573	1.547	1.539	1.623	1.593	1.496	1.610	1.582	1.518
Fe^{2+}	2.451	2.448	2.375	2.407	2.456	2.169	2.151	2.144	2.039	2.125	2.186	2.120	2.111	2.181
Mn	0.036	0.038	0.038	0.038	0.019	0.028	0.028	0.024	0.026	0.024	0.022	0.028	0.026	0.024
Ca	1.893	1.901	1.854	1.850	1.908	1.935	1.935	1.929	0.013	1.923	1.955	1.940	1.946	1.934
Na	0.372	0.365	0.382	0.365	0.408	0.328	0.335	0.335	0.314	0.322	0.301	0.320	0.324	0.330
K	0.297	0.297	0.312	0.310	0.300	0.445	0.399	0.407	0.385	0.398	0.388	0.409	0.383	0.442
Cations	15.612	15.608	15.616	15.595	15.659	15.738	15.699	15.704	15.645	15.679	15.660	15.698	15.678	15.737
Cl	0.268	0.264	0.259	0.266	0.261	0.372	0.364	0.368	0.335	0.349	0.379	0.357	0.333	0.399
X_{Mg}	0.324	0.325	0.340	0.341	0.332	0.424	0.418	0.418	0.443	0.428	0.406	0.432	0.428	0.410

Oxides in wt%, calculation based on 23 oxygens (average of 15-NK and 13-CNK); $X_{Mg} = Mg/(Mg + Fe^{2+})$

Table 18.5 Representative mineral compositions of biotite from the Munali hill area

	Munali hills granite gneiss								Amphibolites					Lusaka granite		Metagabbro	
Sample	MHG2			MHG9			MHG10		MHG5a			MHG5c		LG2		NDG	
	1	3	4	1		3	1	2	1	2	3	1	2	1	2	1	2
SiO_2	34.20	33.70	34.00	34.60	34.60	34.50	34.60	34.40	35.30	35.40	35.50	36.80	35.50	35.70	35.50	39.70	39.20
TiO_2	2.60	2.60	2.46	2.35	3.40	3.40	2.60	2.50	2.54	2.60	2.60	1.72	2.40	1.68	1.73	0.54	0.50
Al_2O_3	16.40	16.40	16.40	17.30	16.50	16.50	16.00	15.90	16.20	16.00	16.10	15.60	16.60	15.30	15.10	12.50	12.50
FeO	29.00	30.50	29.00	25.60	25.90	26.00	28.60	28.90	23.10	22.70	23.10	18.60	22.60	27.60	28.20	22.50	23.30
MnO	0.31	0.40	0.32	0.04	0.10	0.08	0.05	0.05	0.15	0.14	0.16	0.10	0.18	0.41	0.45	0.13	0.12
MgO	4.50	3.40	4.50	7.00	6.20	6.10	5.20	5.30	9.40	9.50	9.70	13.30	9.60	5.80	5.60	7.40	6.90
CaO	0.04	<0.02	0.05	<0.02	<0.02	<0.02	0.02	<0.02	0.04	0.04	0.06	0.02	0.04	0.02	<0.02	11.50	11.40
Na_2O	0.04	0.03	0.03	0.04	0.05	0.04	0.02	0.04	0.08	0.06	0.07	0.07	0.06	0.04	0.06	1.67	1.71
K_2O	9.20	9.10	8.90	9.20	9.30	9.30	8.90	9.10	9.10	9.00	8.60	9.50	9.10	9.10	9.00	1.31	1.40
Cl	0.45	0.59	0.50	0.44	0.43	0.47	0.79	0.82	0.53	0.53	0.53	0.64	0.52	0.64	0.68	1.38	1.61
Total	96.74	96.73	96.16	96.57	96.49	96.39	96.78	97.01	96.44	95.97	96.42	96.35	96.60	96.29	96.32	98.63	98.64
Si	5.438	5.409	5.436	5.397	5.417	5.413	5.483	5.471	5.453	5.474	5.467	5.569	5.450	5.652	5.636	5.938	5.911
Al(IV)	2.562	2.591	2.564	2.603	2.583	2.587	2.517	2.529	2.547	2.526	2.533	2.431	2.550	2.348	2.364	2.062	2.089
Al(VI)	0.505	0.505	0.525	0.571	0.463	0.463	0.461	0.439	0.401	0.397	0.394	0.352	0.449	0.512	0.466	0.146	0.123
Ti	0.313	0.316	0.296	0.276	0.397	0.396	0.310	0.294	0.295	0.302	0.296	0.196	0.277	0.200	0.207	0.061	0.057
Fe^{2+}	3.849	4.103	3.871	3.339	3.398	3.420	3.792	3.839	2.986	2.940	2.976	2.360	2.908	3.659	3.749	2.807	2.942
Mn	0.042	0.055	0.043	0.005	0.014	0.011	0.007	0.006	0.020	0.018	0.021	0.013	0.023	0.055	0.060	0.016	0.015
Mg	1.059	0.809	1.069	1.617	1.451	1.435	1.239	1.245	2.160	2.193	2.215	2.993	2.207	1.359	1.334	1.650	1.554
Ca	0.006	0.002	0.009	0.001	0.002	0.001	0.003	<0.001	0.007	0.007	0.010	0.003	0.006	0.003	<0.001	1.848	1.849
Na	0.011	0.008	0.010	0.012	0.015	0.013	0.006	0.012	0.023	0.018	0.022	0.021	0.017	0.014	0.017	0.483	0.499
K	1.862	1.857	1.804	1.841	1.849	1.854	1.798	1.834	1.785	1.783	1.689	1.826	1.779	1.837	1.829	0.249	0.269
Cations	15.647	15.655	15.627	15.662	15.589	15.593	15.616	15.669	15.677	15.658	15.623	15.764	15.666	15.639	15.662	15.260	15.308
Cl	0.120	0.161	0.137	0.118	0.115	0.130	0.214	0.222	0.139	0.138	0.138	0.163	0.133	0.172	0.183	0.350	0.412
X_{Mg}	0.216	0.165	0.216	0.326	0.299	0.296	0.246	0.245	0.420	0.427	0.427	0.559	0.432	0.271	0.262	0.370	0.346

Oxides in wt%, calculation based on 22 oxygens, $X_{Mg} = Mg/(Mg + Fe^{2+})$

atoms per formula unit (a.p.f.u)), CO_2 (X_{CO2} = 1 – Cl – S a.p.f.u), and meionite composition (Me % = Ca/(Ca + Na + K)). Scapolite from the Munali hills area has a range of compositions from 31–46 EqAn % and 0.37 to 0.50 X_{Cl}. The scapolites are sodium-rich with 27–47 Me % compositions that fall within calcian marialite scapolite compositional group (15< %Me < 50, Fig. 18.4a; Rebbert and Rice 1997). The highest X_{Cl} contents are recorded in the Munali hills granite gneiss sample (MHG10). The compositions of scapolite plot close mid-way between the ideal end-members marialite and meionite, indicating compositions represented by solid solutions between these two end-members and a possible silvialite component $Ca_4[Al_6Si_6O_{24}]SO_4$ (Fig. 18.4b).

Mineral compositions of scapolite in metagabbros from the Copperbelt region (Tembo 1994) have a restricted range between 29 and 38 EqAn % comparable to the compositions of scapolite from the Munali hills area. Compared to those of the Munali hills area, the scapolites from the Copperbelt region have higher X_{Cl} values ranging from 0.61 to 0.84 and data points lie on and above the tie line between the marialite-meionite ideal end-member compositions.

18.5.2 Plagioclase

Plagioclase coexists with scapolite in all samples. The mineral formula was calculated on the basis of 32 oxygens. The plagioclase has a wide compositional range from 13 to 61 anorthite content with lower contents ($An_{23–37}$–oligoclase-andesine) in granite gneisses and higher contents ($An_{36–61}$ –andesine-labradorite) mainly in the amphibolite samples (Fig. 18.4b, Table 18.3). The anorthite contents of plagioclase overlap with coexisting scapolite (Fig. 18.4b). Plagioclase from the non-scapolite bearing granites in the belt, e.g., Lusaka and Nchanga granites, are more sodium-rich with a compositional range of $An_{4–16}$.

18.5.3 Amphiboles

The amphiboles are Cl-bearing ferroan paragasite and magnesian hastingsite. Chlorine contents in pargasite are rather uniform at about 0.26 X_{Cl}, whereas that in hastingsite are slightly higher, ranging from 0.34 to 0.40 X_{Cl}. Similarly, X_{Mg} values range from 0.32 to 0.34 and 0.41 to 0.42 in pargasite and hastingsite, respectively.

18.5.4 Biotite

Biotite mineral formulae were calculated on the basis of 22 oxygens. Biotite was classified into two groups on the basis of Al(IV) a.p.f.u contents and X_{Fe} (Fig. 18.5a). Most biotites have high annite components, except some from one amphibolite sample (MHG5a), which are rich in the phlogopite component. On the X_{Cl}-X_{Mg} diagram (Fig. 18.5b), the biotite (annite-rich) from the metagabbros have the

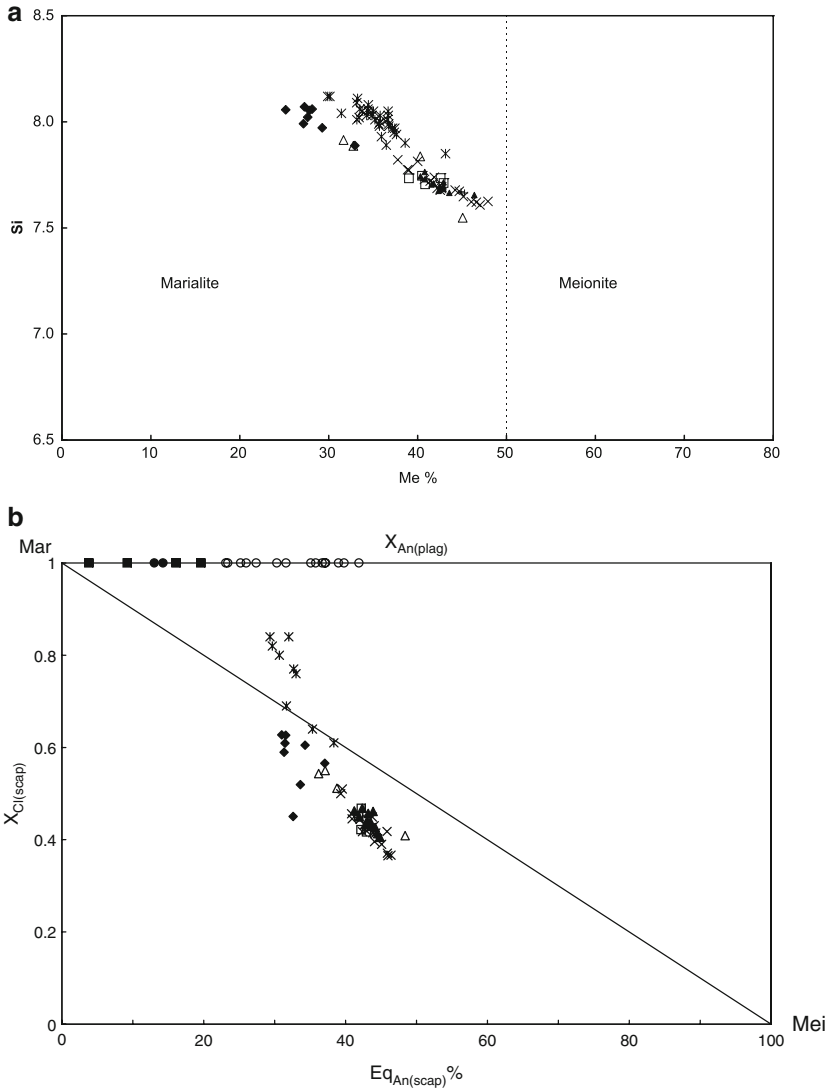

Fig. 18.4 (**a**) Classification of scapolites from the Lufilian–Zambezi belt on the basis of meionite component: Me% = 100 * (Ca/Ca + Na + K). All the scapolite data points plot in the calcian marialite group (After Rebbert and Rice 1997). (**b**) Plot of X_{Cl} versus $EqAn_{(scap)}$ and $X_{An(plag)}$. Scapolite data points from the Munali hills area plot between the three ideal end member tie lines, whereas some data points from the Copperbelt region lie above the ideal compositions. Symbols: ♦MHG10; □ MHG2; +- MHG5a; ▲ MHG5c; ×- MHG9; Δ- NDG; CB- metagabbros; ○ Plag coexisting with scapolite; ● LG-plag; ■- NG-plag

highest Cl contents ranging from 0.6 to 0.9 wt%, whereas biotites from amphibolites have the highest X_{Mg} values. Biotites from non-scapolite bearing rocks such as Lusaka granite also have compositions and Cl contents similar to those coexisting in scapolite-bearing rocks.

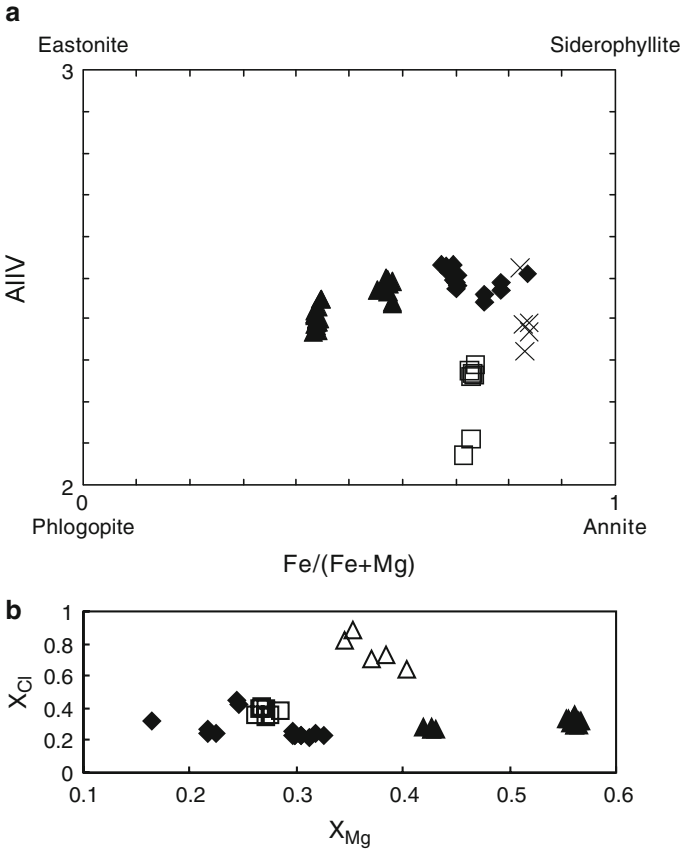

Fig. 18.5 (**a**) Classification of biotite from scapolite and non-scapolite bearing rocks from the Lufilian–Zambezi belt. Most biotites plot in the annite–siderophyllite field, except some from the amphibolitic dyke sample MHG5a. (**b**) Plot of X_{Cl} versus X_{Mg} of biotites from scapolite and non-scapolite bearing rocks from the Lufilian–Zambezi belt. Metagabbros have biotites with the highest Cl contents, whereas some from the amphibolitic dykes have high Mg (the phlogopite-rich biotites in (**a**)). Symbols: ♦ Munali hills granite gneiss; ▲ Amphibolite; Δ Metagabbro; □ Lusaka granite

18.6 Discussion

18.6.1 Scapolite and Fluid Compositions

The NaCl content of a fluid can be estimated from scapolite coexisting with calcite according to the reaction (Ellis 1978):

$$\left(\mathrm{NaCl}\right)_{\mathrm{scp}} + \left(\mathrm{CaCO_3}\right)_{\mathrm{cc}} = \left(\mathrm{CaCO_3}\right)_{\mathrm{scp}} + \left(\mathrm{NaCl}\right)_{\mathrm{fluid}}$$

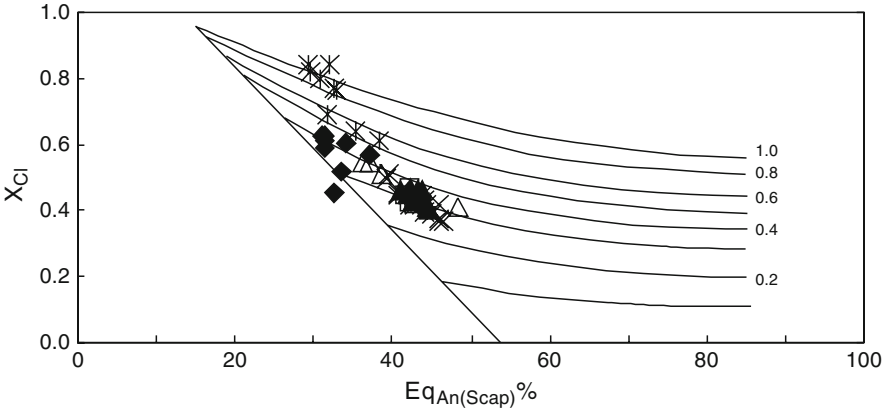

Fig. 18.6 Plot of $X_{Cl,Scap}$-EqAn of scapolites from the Lufilian–Zambezi belt, superimposed on the NaCl salinity curves of Ellis (1978). Data points of scapolite from the Munali hills area indicate salinities ranging from 0.2–0.5 mol, whereas those from the Copperbelt region are unrealistically high. Same symbols as in Fig. 18.4

Ellis (1978) investigated this fluid exchange equilibrium at 750°C and 4 kbar, consistent with metamorphic conditions in the granulite facies. Mora and Valley (1989) outlined the limitations underlying Ellis's expression that are mainly because of thermodynamic mixing properties and inappropriate P–T conditions done by Ellis (1978). In the absence of thermodynamic data different from that of Ellis (1978), we used X_{NaCl} curves of Ellis (1978) to estimate, as a first approximation, the NaCl salinity of coexisting fluids in the belt. The X_{NaCl} in scapolite from the Munali hills area range from 0.2 to 0.5 mol, whereas those from the Copperbelt region (Tembo 1994) are higher and vary from 0.5 to 1 (Fig. 18.6). Salinities in this range are known from areas where evaporite sequences occur (Rich 1979; Roeder 1984; Behr and Horn 1982).

Fluid inclusion studies from carbonate hosted Kabwe Pb–Zn deposit in central Zambia indicate H_2O–NaCl–$CaCl_2$ and H_2O–$MgCl_2$–$CaCl_2$ fluid compositions; salinities ranging from 11 to 31 wt% NaCl equivalent (EQ) and homogenisation temperatures varying from 257°C to 305°C (Kamona 1993). In the Chisamba area, north of Lusaka, H_2O-NaCl fluid inclusions in quartz from vein quartz yielded fluid salinities ranging from 34 to 44 wt% NaCl EQ, and temperatures between 250°C and 350°C (Katongo 1999). These independent fluid inclusion studies indicate relatively high NaCl salinities at conditions consistent with greenschist facies metamorphism, but the host rocks are not scapolite bearing.

Scapolites from both the Munali hills area and Copperbelt region have strikingly similar calcian-marialitic compositions (23–48 Me%), but this may well just be a coincidence, as the two areas are several hundreds of kilometres apart. However, similar compositions were also found with the crude analytical techniques mentioned earlier. However, Munyanyiwa (1990) reported scapolite of mizzonite composition from southern Zambia without providing mineral compositional data.

Experiments by Vanko and Bishop (1982) showed that marialitic scapolite could be formed in fluids with little or no calcite. A minimum salinity for the production

of marialitic scapolite in the absence of calcite is about 0.5 mol NaCl at 700–750°C (Vanko and Bishop 1982), which falls within the salinity range of our results (0.2–0.5 mol NaCl), estimated from the salinity curves of Ellis (1978). Some of the higher X_{NaCl} values in our data set are unrealistic and underscore the limitation of applying Ellis's experimental results to systems of different thermodynamic conditions, as pointed-out by several other authors (e.g., Mora and Valley 1989).

The composition of scapolite in the Munali hills area is independent of the lithology and coexisting mineral phases. The composition of coexisting plagioclase ($An_{23–48}$), which lies within the same compositional range as the anorthite equivalent of the scapolite ($EqAn_{29–48}$), appears to be an important factor in favoring scapolitization, because plagioclase from non-scapolite bearing Lusaka and Nchanga granites is more albite-rich ($An_{5–20}$) than that coexisting with scapolite. Biotite is most commonly used in estimating halogen contents of fluids (Munoz and Swenson 1981) but we found no direct correlation between scapolite and biotite in the Munali hills granite gneiss, especially that Cl-bearing biotite also occurs in non-scapolite bearing Lusaka and Nchanga granites. However, phlogopite-rich biotite, which occurs in equilibrium with scapolite in veinlets in some amphibolites, was evidently formed under similar metamorphic conditions with scapolite. Similarly, the metamorphic Cl-bearing amphiboles also occur in equilibrium with scapolite and probably formed during the same metamorphic event.

18.6.2 Mineral Assemblages and Metamorphism in the Lufilian–Zambezi Belt

In the Lufilian–Zambezi belt, scapolites occur in mineral assemblages that are indicative of amphibolite facies metamorphism. In southern Zambia, amphibolite facies metamorphism is reflected by the scapolite–tremolite–diopside assemblage in calc-silicates, and scapolite–garnet–hornblende assemblage in garnet amphibolites (Simpson et al. 1965; Munyanyiwa 1990; Katongo 1999). However, in the Copperbelt region, Tembo (1994) reported greenschist facies assemblages comprising scapolite–chlorite–epidote–sericite in metagabbros. However, elsewhere around the world, scapolites occur in association with mineral assemblages that are stable at metamorphic conditions ranging from amphibolite to granulite facies (e.g., Vanko and Bishop 1982; Markl and Piazolo 1998; Faryad 2002). In our sample suite, scapolite formed mainly at the expense of plagioclase, especially in the Munali hills granite gneiss, however the scapolite–plagioclase assemblage is stable over a wide range of metamorphic conditions. Breakdown of plagioclase to sericite is indicative of greenschist facies metamorphism, which post-dated scapolitization. In amphibolites, however, scapolite is in equilibrium with both Cl-bearing biotite and amphiboles, suggesting that the assemblage formed during amphibolite facies metamorphism.

The symplectite-like intergrowth of scapolite with quartz (Fig. 18.2b) observed in the Munali hills granite gneiss is not common in most scapolite bearing rocks. Because scapolite invariably replaced plagioclase in most rocks, this texture could have formed

in two ways. Myrmekite-like intergrowths between scapolite and quartz adjacent to K-feldspar are common in most samples, therefore the first and most likely possibility is that scapolite replaced plagioclase, which had already formed myrmekite intergrowth with quartz. The second possibility is that scapolite replaced calcium-rich plagioclase. Since scapolite has less SiO_2 in the crystal lattice than calcium-rich plagioclase, the excess SiO_2 was exsolved after replacement and formed worm-like blebs as inclusions in scapolite, resulting in the symplectite-like intergrowth. A replacement of K-feldspar by scapolite was not found in the investigated samples.

18.6.3 Origin of Scapolite and NaCl-Rich Fluids

The distribution of scapolite in the field is often the best evidence for the origin of this mineral. Several modes of field occurrence that indicate the possible origin of scapolite are proposed. Scapolite distributed as fine-scale interbedded units of scapolite-bearing beds in meta-evaporites suggests strongly for an in-situ salt precursor (e.g., Hietanen 1967; Mora and Valley 1989; Markl and Piazolo 1998). In southern Zambia, most scapolite-bearing marble and calc-silicate rocks probably represent in-situ former evaporitic sequences because metamorphism in most cases was essentially isochemical (Munyanyiwa 1990; Munyanyiwa and Hanson 1988). Any other mode of occurrence is attributed to metasomatism (e.g., Vanko and Bishop 1982). Metasomatic introductions of NaCl fluids are associated with scapolite occurrences in meta-igneous rocks, which otherwise do not contain scapolite. In the Copperbelt region, evidence of former evaporites provides unambiguous precursor for the external source of NaCl-rich fluids for the origin of the scapolite. In the Munali hills and surrounding areas, there is no hard evidence indicating the occurrence of former evaporites in the area. However, Cl-rich scapolite in the Munali hills area, coupled high NaCl salinities of coexisting fluids determined in this study, are indicative of an external source of NaCl-rich fluids from former evaporite horizons in the supracrustal rocks that correlate well with the Katangan metasediments in the Copperbelt region. Thus, the most credible source for NaCl fluids in the Lufilian–Zambezi belt, as previously suggested by many authors, is the dissolution of evaporite horizons in metasedimentary sequences during regional amphibolite facies metamorphism that channeled through fault and shear zones in the area. These investigations show that the study area is of great importance to understand the relation between evaporites and scapolites.

18.7 Summary and Conclusions

We conducted fieldwork in the Munali hills area, in the southern part of the Lufilian–Zambezi belt, and performed petrographic and mineral analyses of scapolite, amphibole, biotite and plagioclase from the Munali hills granite gneiss,

amphibolites and metagabbros, in an effort to evaluate the nature of fluids, their source and attending metamorphic conditions. Results of this study show that:

1. The scapolites from the Munali hills area and from the Copperbelt region have strikingly similar Ca-rich marialite compositions (28–46 Me%), indicating that the mineral formed from hydrothermal fluids from precursor rocks of similar composition.
2. The scapolite in the Munali hills area occurs as pervasive replacement of plagioclase (21–48 X_{An}%) by metasomatic processes and occurs in stable equilibrium with mineral assemblages that are indicative of amphibolite facies metamorphism. The abundance of scapolite throughout the belt suggests that the grade of metamorphism in most parts of the belt was at least amphibolite facies, at which scapolite is more stable than plagioclase in the presence of NaCl-rich fluids.
3. The source of NaCl-rich fluids for the formation of scapolite in the Copperbelt region is evidently from evaporite horizons in the Katangan metasedimentary succession. In the southern part of the belt, including the Munali hills area, there is no direct evidence of the former existence of the evaporite beds. The prevalence of Cl-rich scapolite in the Munali hills area and high NaCl salinities of coexisting fluids, indicate former extensive evaporite successions in the supracrustal rocks that correlate well with the Katangan metasediments in the Copperbelt region.

Acknowledgements We thank the Austrian Academic Exchange Service (ÖAD) for a Ph.D. stipend to C. Katongo. Analytical expenses were supported by the Austrian science Foundation FWF. The co-authors would like to dedicate this paper to the memory of Crispin Katongo, who passed away after a short illness on July 18, 2004, at the age of 38, shortly after completing his PhD at the University of Vienna. We are grateful to three anonymous reviewers, and Prof. Jyotisankar Ray, whose extensive and constructive comments helped to improve this manuscript.

References

Barton CM, Carney JN, Crow MJ, Dunkley PN, Simango S (1991) The geology of the country around Rushinga and Nyamapanda. Bull Geol Surv Zimbabwe 92:220

Bayliss P (1987) Mineral nomenclature: scapolite. Mineralog Mag 41:176

Behr HJ, Horn EE (1982) Fluid inclusion systems in metaplaya deposits and their relationship to mineralization and tectonics. Chem Geol 37:173–189

Binda PL (1994) Stratigraphy of the Zambian Copperbelt orebodies. J Afr Earth Sci 19:251–264

Broderick TJ (1981) The Zambezi metamorphic belt in Zimbabwe. In: Hunter DR (ed) Precambrian of the southern hemisphere. Elsevier, Amsterdam, The Netherlands, pp 739–743

Burnard P, Sweeney MA, Vaughan DJ, Spiro B, Thirwall MF (1993) Sulfur and lead isotope constraints on the genesis of a southern Zambian massive sulphide deposit. Econ Geol 88:418–436

Cahen L, Snelling NL, Delhal J, Vail JR, Bonhomme M, Ledent D (1984) Geochronology and evolution of Africa. Clarendon, Oxford, p 512

Cailteux J, Kampunzu AB (1995) The Katangan tectonic breccias in the Shaba Province (Zaire) and their genetic significance. In: Wendorff M, Tack L (eds) Late Proterozoic belts in Central and Southern Africa. Annales Sciences Géologigues Musée Royal de I´Afrique Centrale 101, Tervuren, pp 49–62

Cailteux J, Binda PL, Katekesha WM, Kampunzu AB, Intiomale MM, Kapenda D, Kaunda C, Ngongo K, Tshiauka T, Wendorff M (1994) Lithostratigraphical correlation of the neoproterozoic Roan Supergroup from Shaba (Zaire) and Zambia, in central African copper-cobalt metallogenic province. J Afr Earth Sci 19:265–278

Cosi M, De Bonis A, Gosso G, Hunziker J, Martinotti G, Moratto S, Robber JP, Ruhlman F (1992) Late Proterozoic thrust tectonics, high pressure metamorphism and uranium mineralisation in the Domes Area, Lufilian Arc, northwestern Zambia. Precambrian Res 58:215–240

Coward MP, Daly MC (1984) Crustal lineaments and shear zones in Africa: their relationship to plate movements. Precambrian Res 24:27–45

Daly MC (1986) Crustal shear zones and thrust belts: their geometry and continuity in central Africa. Philos Trans R Soc Lond A317:111–128

De Swardt AML, Drysdall AR (1964) Precambrian geology and structure in central northern Rhodesia. Mem Geol Surv N Rhodesia 2:82

De Waele B, Fitzsimons ICW, Wingate MTD, Tembo F, Mapani B, Belousova EA (2009) The geochronological framework of the Irumide belt: a prolonged crustal history along the margin of the Bangweulu craton. Am J Sci 309:132–187

Dirks PHGM, Sithole TA (1999) Eclogites in the Makuti gneisses of Zimbabwe: implications for the tectonic evolution of the Zambezi belt in southern Africa. J Metamorph Geol 17:593–612

Drysdall AR, Stillman CJ (1966) Scapolite from the Katanga carbonite rocks of the Lusaka district. Records Geol Soc Zambia 10:20–24

Ellis DE (1978) Stability and phase equilibria of chloride-and carbonate bearing scapolites at 750 °C and 4000 bar. Geochim Cosmochim Acta 42:1271–1281

Evans BW, Shaw DM, Haughton DR (1969) Scapolite stoichiometry. Contrib Mineralog Petrol 24:293–305

Faryad SW (2002) Metamorphic conditions and fluid compositions of scapolite bearing rocks from the Lapis Lazuli deposit at Sare Sang, Afghanistan. J Petrol 13:725–747

Hanson RE, Wilson TJ, Brueckner HK, Onstott TC, Wardlaw MS, Johns CC, Hardcastle KC (1988) Reconnaissance geochronology, tectono-thermal evolution and regional significance of the Middle Proterozoic Choma-Kalomo block, southern Zambia. Precambrian Res 42:39–61

Hanson RE, Wardlaw MS, Wilson TJ, Mwale G (1993) U-Pb zircon ages from the Hook granite massif and Mwembeshi dislocation: constraints on Pan-African deformation and transcurrent shearing in central Zambia. Precambrian Res 63:189–209

Hanson RE, Wilson TJ, Munyanyiwa H (1994) Geologic evolution of the Neoproterozoic Zambezi orogenic belt in Zambia. J Afr Earth Sci 18:135–150

Hargrove US, Hanson RE, Martin MW, Blenkinsop TG, Bowring SA, Walker N, Munyanyiwa H (2003) Tectonic evolution of the Zambezi belt: geochronological, structural and petrographical constraints from northern Zimbabwe. Precambrian Res 123:159–186

Harley SL, Fitzsimons ICW, Buick IS (1994) Reactions and textures in wollastonite-scapolite granulites and their significance for pressure-temperature-fluid histories of high-grade terranes. Precambrian Res 66:309–323

Hietanen AH (1967) Scapolite in the Belt series in the St Joe-Clear water Region, Idaho. Geol Soc Am Spec Pap 86:56

Jackson MAP, Warin ON, Woad GM, Hudec MR (2003) Neoproterozoic allochthonous salt tectonic during the Lufilian orogeny in the Katangan Copperbelt, central Africa. Geol Soc Am Bull 115:314–330

John T, Schenk V, Haase K, Scherer E, Tembo F (2003) Evidence of a Neoproterozoic ocean in south-central Africa from mid-ocean-ridge-type geochemical signatures and pressure-temperature estimates of Zambian eclogites. Geology 31:243–246

Johnson SP, Oliver GJH (2000) Mesoproterozoic oceanic subduction, Island-arc formation and the initiation of back-arc spreading in the Kibaran belt of central southern Africa: evidence from the Ophiolite Terrane, Chewore Inliers, northern Zimbabwe. Precambrian Res 103:125–146

Johnson SP, Fitzsimons ICW, Wingate MTD, Tembo F, Mapani B, Belousova EA (2007) The geochronological framework of the Irumide belt: a prolonged crustal history along the margin of the Bangweulu craton. Am J Sci 309:132–187

Kamona F (1993) The carbonate-hosted Kabwe Pb-Zn deposit, central Zambia. Ph.D thesis, Technical University of Archean, 207 pp

Kampunzu AB, Cailteux J (1999) Tectonic evolution of the Lufilian arc central Africa Copperbelt during Neoproterozoic Pan-African orogenesis. Gondwana Res 2:135–150

Katongo C (1999) Structural and petrographic fabrics in the Chisamba and Kabwe areas, central Zambia: implications for the Late Proterozoic Mwembeshi Dislocation Zone. M.Sc. thesis (unpublished), University of Zambia, 209 pp

Katongo C, Koller F, Kloetzli U, Koeberl C, Tembo F, De Waele B (2004) Petrography, geochemistry and geochronology of key granitoid rocks in the Neoproterozoic-Paleozoic Fufilian-Zambesi belt, Zambia: implications for tectonic setting and regional correlation. J Afr Earth Sci 40:219–244

Key RM, Liyungu AK, Njamu FM, Somwe V, Banda J, Mosley PN, Armstrong RA (2001) The western arm of the Lufilian arc in NW Zambia and its potential for copper mineralisation. J Afr Earth Sci 33:503–528

Mallick DIJ (1966) The stratigraphy and structure of the Mpande Dome, southern Zambia. Trans Geol Soc SA 69:211–230

Markl G, Piazolo S (1998) Halogen-bearing minerals in syenites and high-grade marbles of Dronning Maud Land, Anrtartica: monitors of fluid compositional changes during late-magmatic fluid-rock interaction processes. Contrib Mineralog Petrol 132:246–268

Mendelsohn F (1961) The geology of the Northern Rhodesia copper belt. McDonald, London, p 523

Moecher DP, Essene EJ (1991) Calculations of CO_2 activities using scapolite equilibria: constraints on the presence and composition of fluids phase during high grade metamorphism. Contrib Mineralog Petrol 108:219–240

Moine B, Guilloux L, Audeoud D (1986) Major element geochemistry of host rocks in some sediment-hosted copper deposits. In: Friedrich GH (ed) Geology and metallogeny of copper deposits. Springer, Berlin, pp 443–460

Mora CI, Valley JW (1989) Halogen-rich scapolite and biotite: implications for metamorphic fluid-rock interaction. Am Mineralog 74:721–737

Munoz JL, Swenson A (1981) Chloride-hydroxyl exchange in biotite and estimation of relative HCL/HF activities in hydrothermal fluids. Econ Geol 76:2212–2221

Munyanyiwa H (1985) The geochemistry and metamorphism of calc-silicate rocks, marbles and amphibolites in a portion of the Zambezi belt, southern Zambia. M.Sc. thesis (unpublished) University of Zambia, 193 pp

Munyanyiwa H (1990) Mineral assemblages in calc-silicates and marbles in Zambezi mobile belt: their implications on mineral-forming reactions during metamorphism. J Afr Earth Sci 10:693–700

Munyanyiwa H, Hanson RE (1988) Geochemistry of marbles and calc-silicate rocks in the Pan-African Zambezi belt, Zambia. Precambrian Res 38:177–200

Munyanyiwa H, Hanson RE, Blenkinsop TG, Treloar PJ (1997) Geochemistry of amphibolites and quartzofeldspathic gneisses in the Pan-African Zambezi belt, northwest of Zimbabwe: evidence for bimodal magmatism in a continental rift setting. Precambrian Res 81:179–196

Orville PM (1975) Stability of scapolite in the system Ab-An-NaCl-$CaCO_3$ at 4 kbar and 750°C. Geochim Cosmochim Acta 39:1091–1105

Oterdoom WH, Wenk HR (1983) Ordering and composition of scapolite; field observations and structural interpretations. Contrib Mineralog Petrol 83:330–341

Porada H (1989) Pan-African rifting and orogenesis in southern to equatorial Africa and eastern Brazil. Precambrian Res 44:103–136

Porada H, Berr HJ (1988) Setting and sedimentary facies of late Proterozoic alkali lake (playa) deposits in the southern Damara belt of Namibia. Sed Geol 58:171–194

Porada H, Berhorst V (2000) Towards a new understanding of the Neoproterozoic-Early Palaeozoic Lufilian and northern Zambezi belts in Zambia and the Democratic Republic of Congo. J Afr Earth Sci 30:727–771

Pouchou J, Pichoir F (1991) Quantitative analysis of homogeneous or stratified microvolumes applying the model "PAP". In: Heinrich KFJ, Newbury DE (eds) Electron probe quantitation. Plenum, New York, pp 31–75

Rebbert CR, Rice JM (1997) Scapolite-plagioclase exchange: Cl-CO_3 scapolite solution chemistry and implications for peristerite plagioclase. Geochim Cosmochim Acta 61:555–567

Rich RA (1979) Fluid inclusion evidence of Silurian evaporites in southern Vermont. Geol Soc Am Bull 90:1628–1643

Roeder E (1984) Low-medium grade metamorphic environments. Mineralog Soc Am Rev Mineral 12:413–472

Simpson JG, Stillman CJ (1963) Metamorphism and reactions phenomena in gabbros of the Mwembeshi and Lusaka areas. Records Geol Surv Zambia 9:10–14

Simpson JG, Drysdall AR, Lambert HH (1965) The geology and groundwater resources of the Lusaka area: explanation of degree sheet 1528, NW quarter. Rep Geol Surv N Rhodesia 16:59

Smith AG (1963) The geology of the country around Mazabuka and Kafue: explanation of degree sheets 1527, SE quarter and 1528 SW quarter. Rep Geol Surv N Rhodesia 2:32

Teertstra DK, Sherriff BL (1997) Substitution mechanisms, composition trends and the end-member formulae of scapolite. Chem Geol 136:233–260

Tembo F (1994) The geology, geochemistry and tectonic significance of metagabbroic rocks in the Lufilian Arc of Zambia. Ph.D thesis, University of Göttingen, Cuvillier Verlag, Göttingen, 118 pp

Tembo F, Kampunzu AB, Porada H (1999) Tholeiitic magmatism associated with continental rifting in the Lufilian belt of Zambia. J Afr Earth Sci 28:403–425

Unrug R (1983) The Lufilian arc: a microplate in the Pan-African collision zone of the Congo and Kalahari cratons. Precambrian Res 21:181–196

Unrug R (1996) The assembly of Gondwanaland. Episodes 19:11–20

Vanko DA, Bishop FC (1982) Occurrence and origin of marialitic scapolite in Humboldt Lapolith, N.W Nevada. Contrib Mineralog Petrol 81:277–289

Vinyu ML, Hanson RE, Martin MW, Bowring SA, Jelsma HA, Krol MA, Dirks PHGM (1999) U-Pb and $^{40}Ar/^{39}Ar$ geochronological constraints on tectonic evolution of the eastern part of the Zambezi orogenic belt, northeast Zimbabwe. Precambrian Res 98:67–82

Vrána S (1978) Metamorphic patterns in Zambia and their bearing on problems of Zambian tectonic history. Precambrian Res 5:127–130

Vrána S, Barr MWC (1972) Talc-Kyanite-quartz schists and other high-pressure assemblages from Zambia. Mineralog Mag 38:837–846

Vrána S, Prasad R, Fediuková E (1975) Metamorphic kyanite eclogites in the Lufilian arc of Zambia. Contrib Mineralog Petrol 51:1–22

Wendorff M (2000) Genetic aspects of the Katangan megabreccias: Neoproterozoic of central Africa. J Afr Earth Sci 30:703–715

Weil AB, Van der Voo R, MacNiocall C, Meert JG (1998) The Proterozoic supercontinent Rodinia: paleomagnetically derived reconstructions for 1100–800 Ma. Earth Planet Sci Lett 154:13–24

Wilson T, Hanson RE, Wardlaw MS (1993) Late proterozoic evolution of the Zambezi belt, Zambia: implications for the regional Pan-African and shear displacements in Gondwana. In: Findlay RH, Unrug R, Banks MR, Veevers JJ (eds) Gondwana Eight: assembly, evolution and dispersal. Balkema, Rotterdam, The Netherlands, pp 69–82